DOI: 10.1002/chem.200902463

Size-Tunable Synthesis of Monodisperse Water-Soluble Gold Nanoparticles with High X-ray Attenuation

Zhijiang Wang,[a] Lina Wu,[b] and Wei Cai*[a]

The use of functional gold nanoparticles in biology is one of the fast-moving and exciting fields in nanotechnology.[1–8] Methods that enable the synthesis of highly stable gold nanoparticles with controlled size or shape has received a widespread research effort because the properties, such as optical, magnetic, electronic, and catalytic activities, are all dimensionally sensitive.[9–14] To obtain high-quality gold nanoparticles, previous studies have explored the utility of citrate, thiolates, phosphanes, amines, carbonyls, dendrimers, and surfactant ligands to stabilize gold nanoparticles in solution.[15] Particularly, thiolate-capped gold nanoparticles are of special interest because the organothiolate isolable monolayer-protected gold products exhibit superb stability to air exposure, long-term storage, and concentration extremes.[16,17]

Among the methods used to prepare thiolate-capped gold nanoparticles, including ligand-exchange procedures and direct synthesis, the Brust synthesis is believed to be the simplest and provides a gram-scale approach.[18,19] This synthesis proceeds in three steps, as shown in Equations (1)–(3):[20–24]

$$Au^{III} + 3SR \rightarrow Au^{I}SR + RSSR \quad (1)$$

$$n Au^{I}SR \rightarrow (-Au^{I}/SR-)_n (polymer) \quad (2)$$

$$4(-Au^{I}/SR-)_n + n BH_4^- \rightarrow Au_x(SR)_y + 2nH_2 \quad (3)$$

[a] Z. Wang, Prof. W. Cai
School of Materials Science and Engineering
Harbin Institute of Technology
Harbin, 150001 (P.R. China)
Fax: (+86) 451-86418649
E-mail: weicai@hit.edu.cn

[b] L. Wu
School of Chemical Engineering and Technology
Harbin Institute of Technology
Harbin, 150001 (P.R. China)

Supporting information for this article is available on the WWW under http://dx.doi.org/10.1002/chem.200902463.

The first step [Eq. (1)] involves the reduction of Au^{III} salt to Au^{I} by thiols. Next, Au^{I} forms a polymeric structure ($[Au^{I}SR]_n$) in which Au^{I} ions have a coordination number of two and are bridged by the thiolate sulfur atom [Eq. (2)]. The third step [Eq. (3)] involves further reducing the Au^{I}–SR complexes to Au^{0} by $NaBH_4$. Previous studies have shown that the reaction behavior of gold formation by this synthesis is consistent with a nucleation–growth process.[23] The biphasic method is valued for obtaining high-quality gold nanoparticles with a narrow size distribution because of the function of the phase-transfer reagents (e.g., TOAB = tetraoctylammonium bromide) and the reaction occurring at the toluene/water interface. However, the gold nanoparticles obtained are insoluble in water and have poor biocompatibility. The green single-phase method in which water-soluble gold nanomaterials are produced has great prospective applications in biosciences, but often fails to yield products of equal merit due to the poor understanding of the formation mechanism of monodisperse nanoparticles.[19] To date, most modified procedures to synthesize water-soluble, thiolate-capped gold nanoparticles still suffer from production in broad size distributions, and the monodisperse nanoparticles have to be separated through a subsequent complex size-selection process, such as chromatography,[25] chemical etching,[26] and diafiltration.[27] The difficulty in preparing high-quality, water-soluble nanoparticles has become a major obstacle to practical applications for gold nanomaterials.

Herein, we describe the synthesis of highly stable, monodisperse, water-soluble gold nanoparticles by controlling the nucleation and growth of the gold nuclei. This is done through the green single-phase method without going through a laborious size-sorting process. This process can produce high-quality gold nanoparticles with tunable core sizes. The gold nanoparticles prepared exhibit a much higher X-ray attenuation than commercial computed tomography (CT) iodinated contrast agents.

The procedure to synthesize water-soluble gold nanoparticles is illustrated in Scheme 1. An important discovery from this work is that both forming homogeneous Au^{0} nuclei and

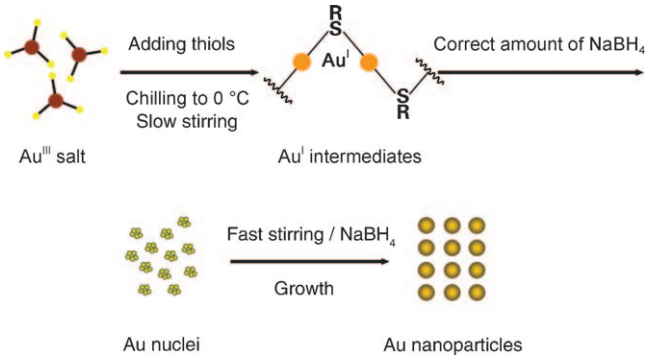

Scheme 1. A schematic illustration of the formation of monodisperse gold nanoparticles.

keeping a uniform growth rate for every nucleus are crucial to producing monodisperse, thiolate-capped gold nanoparticles, which can be fulfilled by controlling the reaction kinetics.

For a description of a typical experiment, see the Experimental Section. Figure 1 shows that the 6.6 nm-sized gold nanoparticles have been successfully prepared. Due to their high monodispersity, they predominantly organize to form well-ordered superlattices on an amorphous carbon-coated Cu TEM grid. The gold nanoparticles isolated as powder (45 mg, ≈90% yield based on gold atom) can be easily dispersed in water (≈60 mg mL^{-1}, at pH 7.0) and stored for months because of the ω-carboxylic acid functionalized alkanethiolate as the protecting ligands (Figures S1–S5 in the Supporting Information).

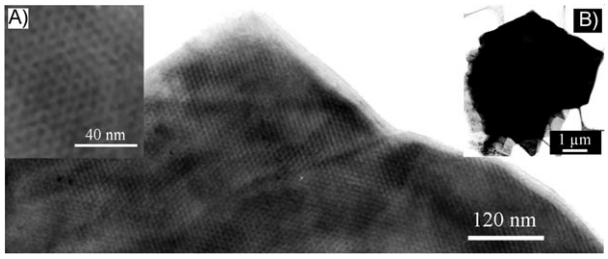

Figure 1. TEM images of a nanocrystal superlattice of 6.6 nm-sized Au nanoparticles. The insets show the magnified image (A) with scale bar of 40 nm and the low-magnification image (B).

The homogeneous Au^0 nuclei are achieved by controlling the size distribution of Au^I intermediates in a narrow range. The 6.6 nm-sized gold nanoparticles are prepared by narrowing the size of Au^I intermediates in the range of 1–21 μm, which are reached by adjusting the stirring speed at low speeds. If the Au^I intermediates are extended to 0.1–150 μm, the polydisperse gold nanoparticles with the core sizes 2–15 nm are produced. The UV/Vis absorption spectrum is characterized by a broad plasmon absorption band, and the maximum shifts to a longer wavelength (Figure 2 and Figure S6 in the Supporting Information). Analyzing the Au^0 nuclei formed by electrospray ionization mass spectrometry, we observed that the gold nanoclusters composed of 12–14 atoms are dominantly yielded from the Au^I intermediates 1–21 μm in size. In contrast, the Au^I intermediates 0.1–150 μm in size produce Au^0 nuclei of a mixture of different cluster sizes from 12 to 55 atoms (see Figure 3; details of the mass assignments are depicted in the Supporting Information). The number of gold atoms contained in the nuclei is dependent on the amount of Au ions in close proximity.[28] The narrow-sized Au^I intermediates have a similar polymeric structure. In this case, the homogeneous nuclei can be synthesized. At the same time, as the core size of a particle decreases, the ratio of the surface atoms to the bulk atoms dramatically increases. There is a strong driving force to minimize the surface free energy by changing the particle structure or reconstructing the surface structure. The strong force results in the formation of "magic number" metal

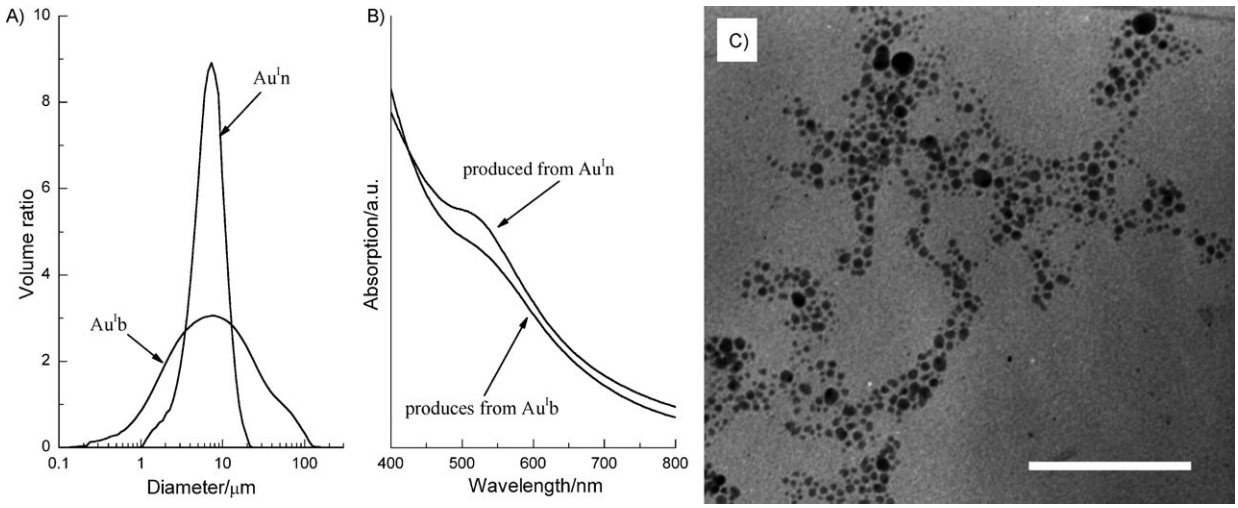

Figure 2. The size distributions of the Au^I intermediates (A), and UV/Vis absorption spectra of the Au nanoparticles formed (B), as well as the TEM image of nanoparticles produced from Au^I_b (scale bar = 100 nm; C). The subscript "n" and "b" designate the Au^I intermediates in the narrow size of 1–21 μm and in the broad size of 0.1–150 μm.

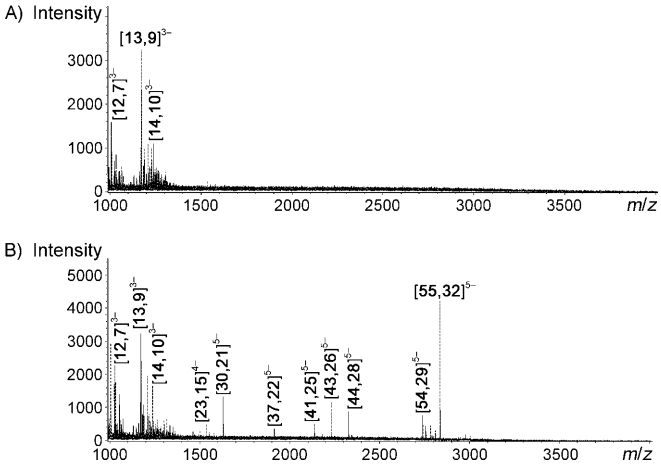

Figure 3. Mass spectra of gold nuclei produced from Au^I intermediates in the sizes of 1–21 μm (A) and in the sizes of 0.1–150 μm (B). The mass peaks are assigned as $[Au_n(SCH_2CH_2COOH)_m - pH^+]^{p-}$, which are denoted as $[n, m]^{p-}$.

nuclei, which are composed of discrete numbers of metal atoms. This is also beneficial to form homogeneous gold nuclei. Furthermore, low temperature is employed in the reaction, which can lead to the formation of less polydisperse gold nanoclusters.[29–32]

The activation energy for the nucleation process is much higher than that for the particle growth,[33] therefore, Au^I intermediates in solution are preferentially reduced on the surface of existing Au^0 nuclei rather than independently forming new particles. This can be evidenced by the seed-mediated growth. In our experiment, to prevent additional nucleation and ensure every nucleus had a uniform growth rate, the stirring speed in the growth stage was changed to a high speed ($\approx$1300 rpm). This is done to ensure the Au^I intermediates have sufficient contact with the formed gold nuclei, and that the flux of the intermediates is equally supplied to every nucleus. If the stirring rate is decreased to $\approx$700 rpm, there is a difference in the flux of Au^I intermediates supplied to the nuclei. In this case, the dispersity of gold nanoparticles produced (core sizes in the range of 3.6–9.6 nm; shown in Figure S8 in the Supporting Information) is worse than that prepared at a higher speed, but is still better than that synthesized from the Au^I intermediates in a broad size distribution.

Subsequently, we synthesized the gold nanoparticles by adding $NaBH_4$ solution at the rate of 0.07, 0.05, and 0.02 mL s^{-1} in the growth step. As shown in Figure 4, the core sizes of gold nanoparticles can be tuned from 8 to 12 nm by varying the rate of addition of borohydride reductant without losing the narrow dispersity characteristic. In general, the average core diameters of nanoparticles prepared by the Brust synthesis are in the range of 0.8–8 nm.[19] Through the synthetic route described herein, the 12 nm monodisperse gold nanoparticles can be prepared.

The X-ray attenuation of the water-soluble gold nanoparticles prepared is examined on a CT scanner and compared with a commercial iodinated contrast agent, Ousu. Figure 5

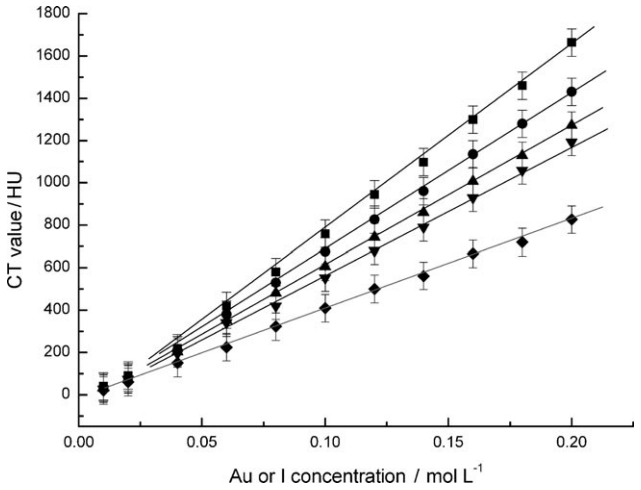

Figure 5. X-ray attenuation and concentration relation of gold nanoparticles 6.6 (■), 8 (●), 10 (▲), and 12 nm (▼) in size, and the Ousu iodinated contrast agent (◆).

shows that the gold nanoparticles exhibit a much higher X-ray attenuation than the Ousu agent at the same concentrations. This could be attributed to the higher theoretical X-ray absorption coefficient of gold compared with iodine (5.16 and 1.94 cm^2 g^{-1}, respectively, at 100 keV).[34] Meanwhile, it can be observed that the X-ray attenuation increased when the core sizes of the gold nanoparticles decreased from 12 to 6.6 nm, which is ascribed to small gold nanoparticles having a larger gold surface area. The X-ray attenuation is dependent on the target area, therefore, the smaller gold nanoparticles exhibit a more striking X-ray attenuation. As is well known, reliable application performance requires consistent properties. Even though the pre-

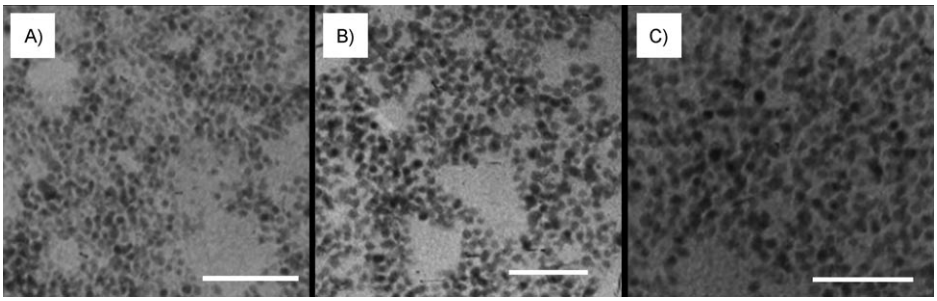

Figure 4. TEM images of different-sized gold nanoparticles produced by varying the adding rate of $NaBH_4$ A) at 0.07 mL s^{-1} with core sizes of (8.0 ± 0.7) nm, B) at 0.05 mL s^{-1} with core sizes of (10.0 ± 0.9) nm, and C) at 0.02 mL s^{-1} with core sizes of (12.0 ± 1.0) nm. All scale bars are 100 nm.

pared gold nanoparticles are stored in the powder state for as long as 14 months, there is still no obvious difference observed in their X-ray attenuation (Figure S9 in the Supporting Information). The performance of the gold nanoparticles prepared and the inherent biocompatibility of the water-soluble gold nanoparticles[35] mean that they have great potential for applications as robust contrast agents for CT scanning. Furthermore, the ω-carboxylic acid functionalized gold nanoparticles can be easily linked with targeting molecules and drug molecules, which may have the dual function of not only increasing the efficiency of CT imaging, but also curing the disease in situ.

In summary, a facile, green method has been developed to synthesize highly stable, monodisperse, water-soluble gold nanoparticles with high X-ray attenuation by controlling the reaction kinetics to form homogeneous Au^0 nuclei and ensure that every nucleus keeps a uniform growth rate. This reported strategy paves the way to preparing high-quality gold nanoparticles with various functionalities, and can accelerate the practical applications of gold nanomaterials in biology.

Experimental Section

Chemicals: MPA ($\geq$99%) and $NaBH_4$ (99%) from Aldrich, and $HAuCl_4 \cdot 3H_2O$ (99.99%, ACS reagent grade) from Alfa were used as received. Iohexol-300 (Ousu 300 mg mL^{-1}) was purchased from Yangtze River Pharmacy Group Co., China. HPLC-grade methanol was used as received. Deionized water of high resistivity (18.2 MΩ cm) was obtained through a TKA GenPure ultrapure water system. All glassware was thoroughly cleaned with aqua regia ($HCl/HNO_3 = 3:1$ vol%), rinsed with ultrapure water, and then dried in an oven prior to use.

Synthesis of gold nanoparticles: For a typical preparation of 6.6 nm-sized gold nanoparticles, $HAuCl_4 \cdot 3H_2O$ (0.0985 g, 0.25 mmol) dissolved in deoxygenated methanol (10 mL) was introduced into a 100 mL three-neck round-bottom flask. The solution was cooled to 0 °C and purged with N_2. Then, MPA (0.2 mL, 3 equiv versus the moles of gold) dissolved in deoxygenated water (10 mL) was added with mechanical stirring at a low speed ($\approx$100 rpm). The deep yellow solution turned to cloudy white, indicating the formation of Au^I–thiol intermediates. After being stirred for over 2 h, the stirring speed was changed to a higher speed ($\approx$1300 rpm), and an aqueous solution of $NaBH_4$ (0.0946 g, 10 equiv versus the moles of gold, freshly prepared in 4 mL ice-cold deoxygenated water) was added. First, 0.05 mL of the aqueous solution of $NaBH_4$ ($\approx$0.125 mole versus that of gold) was quickly added all at once. After 10 s, the rest of the aqueous solution of $NaBH_4$ was added at a set rate of 0.08 mL s^{-1}. The pH value of the solution gradually increased with the addition of $NaBH_4$. The final pH value of the reaction solution was 8.3; this was owing to the hydrolysis of $NaBH_4$.[22] The reaction was allowed to proceed for 1 h. The crude products were precipitated with methanol and washed twice with 30% (v/v) water/methanol as well as three times with methanol to remove the inorganic (Na, Cl, B), unbound MPA and organic impurities. Finally, the products were dried in the vacuum oven (less than 5×10^{-3} Torr) without exceeding 25 °C for a further 12 h, giving 45 mg of powder.

Separation of gold nuclei: Au^I–MPA complexes and unreacted MPA molecules were removed through centrifugal filtration (15000 g) of the mixture by using a filter with a molecular weight cutoff value of 10000 Da. Then, the solution was precipitated with methanol and washed twice with 20% (v/v) water/methanol as well as three times with methanol. The complete removal of MPA molecules was confirmed by mass spectrometry, and complete removal of residual Au^I ions was verified when the color of the sample solution did not change to black after treatment with a solution of $NaBH_4$.

Characterization: TEM images of gold nanoparticle samples were obtained on Philips CM12 and CM20 electron microscopes operated at 120 and 200 keV, respectively. TEM samples were prepared by dropping the diluted solution (pH 7.0) onto amorphous carbon-coated copper grids and drying in the air for 4 h. XPS data were obtained by using a Thermo Scientific K-Alpha Spectrometer equipped with a monochromatic $Al_{K\alpha}$ X-ray source. SEM images were taken on an FEI Quanta 200F scanning electron microscope. An energy-dispersive X-ray (EDX) spectrometer attached to the FEI Quanta 200F provided in situ determinations of the compositions of the as-synthesized solids. The samples were not sputtered with platinum or gold to reduce charging effects. Mass spectra were acquired on a Bruker micrOTOFQ mass spectrometer, which was accurately calibrated and equipped with an electrospray ionization source. The mass analysis was performed in the negative ion mode. Samples were infused at a flow rate of 180 μL h^{-1}. The ion transfer time was set to 160 μs. HPLC-grade methanol was the solvent and was used as received. The size distribution of Au^I intermediates was determined by laser diffraction (Malvern Mastersizer S, Malvern Instruments, UK). UV/Vis absorption spectra were performed on a calibrated spectrophotometer (Cary 4000, Varian) at room temperature. FTIR spectra were recorded on a Perkin–Elmer Spectrum One spectrometer. CT measurement was carried out by employing a Toshiba Aquilion 64 CT Scanner with 400 mA and 120 kVp. Scanning was performed in the transverse axial plane using a slice thickness 0.5 mm. A uniform region of interest was carefully placed over the center of each vial containing the gold nanoparticles dispersion and iodinated contrast agent to measure attenuation values.

Acknowledgements

The authors thank Dr. Kezheng Wang for his help with the CT measurement. This work was supported by the Excellent Youth Foundation of Heilongjiang Province of China (No. JC200715).

Keywords: computed tomography agents · gold · nanoparticles · nucleation · X-ray attenuation

[1] T. A. Taton, C. A. Mirkin, R. L. Letsinger, *Science* **2000**, *289*, 1757–1760.
[2] N. L. Rosi, D. A. Giljohann, C. S. Thaxton, A. K. R. Lytton-Jean, M. S. Han, C. A. Mirkin, *Science* **2006**, *312*, 1027–1030.
[3] X. M. Qian, X. H. Peng, D. O. Ansari, Q. Yin-Goen, G. Z. Chen, D. M. Shin, L. Yang, A. N. Young, M. D. Wang, S. M. Nie, *Nat. Biotechnol.* **2008**, *26*, 83–90.
[4] P. Ghosh, G. Han, M. De, C. K. Kim, V. M. Rotello, *Adv. Drug Delivery Rev.* **2008**, *60*, 1307–1315.
[5] S. Lee, E. J. Cha, K. Park, S. Y. Lee, J. K. Hong, I. C. Sun, S. Y. Kim, K. Choi, I. C. Kwon, K. Kim, C. H. Ahn, *Angew. Chem.* **2008**, *120*, 2846–2849; *Angew. Chem. Int. Ed.* **2008**, *47*, 2804–2807.
[6] S. Bi, Y. M. Yan, X. Y. Yang, S. S. Zhang, *Chem. Eur. J.* **2009**, *15*, 4704–4709.
[7] S. Dhar, E. M. Reddy, A. Shiras, V. Pokharkar, B. L. V. Prasad, *Chem. Eur. J.* **2008**, *14*, 10244–10250.
[8] D. Kim, S. Park, J. H. Lee, Y. Y. Jeong, S. Jon, *J. Am. Chem. Soc.* **2007**, *129*, 7661–7665.
[9] S. W. Chen, R. S. Ingram, M. J. Hostetler, J. J. Pietron, R. W. Murray, T. G. Schaaff, J. T. Khoury, M. M. Alvarez, R. L. Whetten, *Science* **1998**, *280*, 2098–2101.
[10] G. Hodes, *Adv. Mater.* **2007**, *19*, 639–655.
[11] C. J. Xu, G. A. Tung, S. H. Sun, *Chem. Mater.* **2008**, *20*, 4167–4169.
[12] T. K. Sham, *Int. J. Nanotechnol.* **2008**, *5*, 1194–1246.

[13] K. W. Kho, Z. X. Shen, H. C. Zeng, K. C. Soo, M. Olivo, *Anal. Chem.* **2005**, *77*, 7462–7471.
[14] Z. J. Wang, W. Cai, J. H. Sui, *ChemPhysChem* **2009**, *10*, 2012–2015.
[15] M. C. Daniel, D. Astruc, *Chem. Rev.* **2004**, *104*, 293–346.
[16] M. Brust, M. Walker, D. Bethell, D. J. Schiffrin, R. Whyman, *J. Chem. Soc. Chem. Commun.* **1994**, 801–802.
[17] M. Brust, J. Fink, D. Bethell, D. J. Schiffrin, C. Kiely, *J. Chem. Soc. Chem. Commun.* **1995**, 1655–1656.
[18] M. Giersig, P. Mulvaney, *Langmuir* **1993**, *9*, 3408–3413.
[19] J. A. Dahl, B. L. S. Maddux, J. E. Hutchison, *Chem. Rev.* **2007**, *107*, 2228–2269.
[20] T. G. Schaaff, G. Knight, M. N. Shafigullin, R. F. Borkman, R. L. Whetten, *J. Phys. Chem. B* **1998**, *102*, 10643–10646.
[21] D. V. Leff, P. C. Ohara, J. R. Heath, W. M. Gelbart, *J. Phys. Chem.* **1995**, *99*, 7036–7041.
[22] S. H. Chen, K. Kimura, *Langmuir* **1999**, *15*, 1075–1082.
[23] A. C. Templeton, M. P. Wuelfing, R. W. Murray, *Acc. Chem. Res.* **2000**, *33*, 27–36.
[24] C. J. Ackerson, P. D. Jadzinsky, R. D. Kornberg, *J. Am. Chem. Soc.* **2005**, *127*, 6550–6551.
[25] G. H. Woehrle, J. E. Hutchison, *Inorg. Chem.* **2005**, *44*, 6149–6158.
[26] Y. Shichibu, Y. Negishi, H. Tsunoyama, M. Kanehara, T. Teranishi, T. Tsukuda, *Small* **2007**, *3*, 835–839.
[27] S. F. Sweeney, G. H. Woehrle, J. E. Hutchison, *J. Am. Chem. Soc.* **2006**, *128*, 3190–3197.
[28] R. P. Briñas, M. H. Hu, L. P. Qian, E. S. Lymar, J. F. Hainfeld, *J. Am. Chem. Soc.* **2008**, *130*, 975–982.
[29] M. J. Hostetler, J. E. Wingate, C. J. Zhong, J. E. Harris, R. W. Vachet, M. R. Clark, J. D. Londono, S. J. Green, J. J. Stokes, G. D. Wignall, G. L. Glish, M. D. Porter, N. D. Evans, R. W. Murray, *Langmuir* **1998**, *14*, 17–30.
[30] R. L. Donkers, D. Lee, R. W. Murray, *Langmuir* **2004**, *20*, 1945–1952.
[31] J. B. Tracy, G. Kalyuzhny, M. C. Crowe, R. Balasubramanian, J. P. Choi, R. W. Murray, *J. Am. Chem. Soc.* **2007**, *129*, 6706–6707.
[32] M. Zhu, E. Lanni, N. Garg, M. E. Bier, R. Jin, *J. Am. Chem. Soc.* **2008**, *130*, 1138–1139.
[33] S. Auer, D. Frenkel, *Nature* **2001**, *409*, 1020–1023.
[34] http://physics.nist.gov/PhysRefData/XrayMassCoef.
[35] N. Lewinski, V. Colvin, R. Drezek, *Small* **2008**, *4*, 26–49.

Received: September 7, 2009
Published online: December 23, 2009

